ELEVENTH INTERNATIONAL CONFERENCE ON INTERGRANULAR AND INTERPHASE BOUNDARIES 2004

JOURNAL OF MATERIALS SCIENCE **40** (2005) 3137–3142

Stress-induced facet coarsening in a $\Sigma 7\{45\bar{1}0\}$ symmetrical tilt grain boundary in an alumina bicrystal

S. HANYU, H. NISHIMURA, K. MATSUNAGA, T. YAMAMOTO*, Y. IKUHARA
*Institute of Engineering Innovation (*Department of Materials Science), The University of Tokyo, 2-11-16 Yayoi, Bunkyo-ku, Tokyo 113-8656, Japan*
E-mail: matu@sigma.t.u-tokyo.ac.jp

A. M. GLAESER
Department of Materials Science and Engineering, University of California, Berkeley, 319 Hearst Memorial Mining Building, MC1760, Berkeley, CA 94720-1760, USA

Grain boundary sliding and migration often accompany high temperature deformation in alumina, however the studies of the sliding and migration behavior of individual boundaries in bicrystals during deformation are extremely limited.

In this study a single grain boundary in an alumina bicrystal was deformed at high temperature (1450°C) at a constant strain rate (2×10^{-6}/s). Evolution of the grain boundary structure during deformation was monitored using optical microscopy. Movement of micron-sized facets inclined to the grain boundary plane led to the facet coarsening and produced macroscopically "curved" regions along the grain boundary.

HRTEM studies reveal nanoscale analogues to such "curved" segments, which appear to contain nanoscale facets. Rumpling of the grain boundary during early stages of deformation may assist the nucleation of facets inclined to the original grain boundary plane. Macroscopic facets may develop by either growth and coarsening of atomic-height irregularities initially in the grain boundary or from atomic-height ledges formed during deformation.

1. Introduction

Polycrystalline alumina has been widely used as a structural material. The properties of grain boundaries not only influence the microstructure and properties developed during processing, but also the stability of these properties during high-temperature service. Grain boundaries in polycrystalline materials, of which alumina serves as just one example, have different properties depending on their grain boundary character (grain boundary misorientation and grain boundary plane orientation). During high-temperature deformation of alumina, grain boundary sliding and grain boundary migration are important phenomena [1, 2]. As a result, from a basic science perspective, it is critical to study the relationship between grain boundary character and grain boundary properties in alumina. Experiments using bicrystals allow systematic studies of such relationships because the grain boundary character can be controlled, systematically varied, and duplicated as necessary to span a wide range of misorientation space, use conditions, or both.

To date, experiments employing bicrystals have been adopted to investigate grain boundary structures and mechanical properties in metals [3–7]. The coincidence site lattice (CSL) [8] and displacement shift complete (DSC) lattice have been used to specify and describe the grain boundary structures and the related properties [9]. The CSL is characterized by the Σ parameter, which indicates the volume fraction ratio of primitive lattice and CSL lattice formed at the boundary, and the DSC lattice is formed by constructing lines that intersect all lattice sites in one crystal to all the lattice sites in the other crystal. It has been known that mechanical properties, energies and atomic core structures of symmetrical grain boundaries are dependent on the grain boundary characters. In experiments on metal systems, deep grain boundary energy cusps are often observed for small Σ values. It has also been reported that grain boundary sliding is more difficult in samples with small Σ than larger Σ grain boundaries [3]. Fewer bicrystal experiments have been performed in ceramic systems than in metallic system, however, studies have been performed using Al_2O_3 [10–19], ZrO_2 [20–24], TiO_2 [25, 26], MgO [27], and NiO [28] to reveal the atomic structures and to assess the energies of special grain boundaries. For grain boundaries in

*Author to whom all correspondence should be addressed.

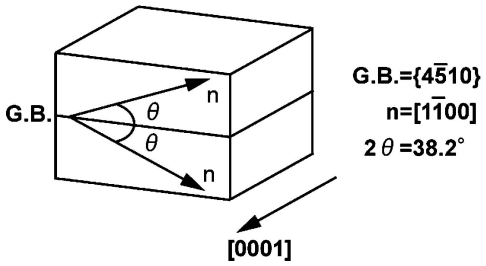

Figure 1 Schematic of an alumina bicrystal fabricated in this study. The crystallographic misorientation is Σ7 and the grain boundary plane corresponds to {4$\bar{5}$10}.

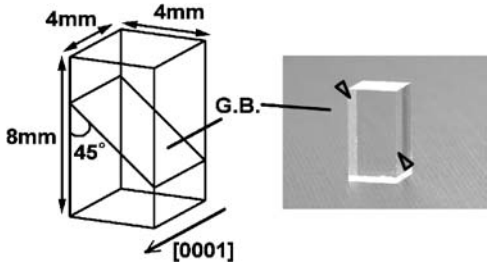

Figure 2 Schematic illustration of the bicrystal for compression tests. A basal plane is parallel to the compressive axis, and the grain boundary plane is inclined by 45° with respect to the axis.

alumina, atomic structures have been experimentally analyzed by HRTEM (High Resolution Transmission Electron Microscopy) and theoretically modeled using static lattice calculations [17, 29, 30].

In the study, an alumina bicrystal containing a single well-defined grain boundary was deformed at high temperature, and the effects of stress and strain on the grain boundary were examined using optical and transmission electron microscopy to assess microstructural changes at multiple length scales.

2. Experimental procedures

2.1. Fabrication of alumina bicrystal

High-purity (>99.99%) α-alumina single crystals (sapphire) were used to fabricate an alumina bicrystal. Two sapphire blocks were cut with a diamond saw to produce cut surfaces parallel to [0001] and inclined 19.1° from the [1$\bar{1}$00] direction as shown schematically in Fig. 1. The resulting sapphire blocks were $6 \times 12 \times 15$ mm^3. Prior to bonding, the cut surfaces were polished mechano-chemically using colloidal silica to obtain mirror finishes. The two crystals were stacked with their polished {4$\bar{5}$10} surfaces in contact and their [0001] directions parallel to one another. The blocks were diffusion bonded at 1500°C, for 10 h in air to produce a bicrystal. The sample geometry described in Fig. 1 yields a Σ7, 38.2° [0001] symmetrical tilt grain boundary, hereafter referred to as a Σ7{4$\bar{5}$10} boundary. The size of the resulting bicrystal was $12 \times 12 \times 15$ mm^3 with the grain boundary at the sample's mid-plane.

2.2. Compression tests

To prepare samples for high-temperature compression testing, the bicrystal was cut using a diamond saw to produce multiple $4 \times 4 \times 8$ mm^3 samples with the grain boundary inclined 45° to the compression axis to maximize the shear stress acting on the grain boundary. In contrast, the {0001} plane (basal plane) was aligned parallel to the compression axis to prevent basal slip (Fig. 2). Scratches traversing the grain boundary were introduced into the {0001} surfaces of the specimen using a 9 μm diamond slurry to provide a means of monitoring the amount of the grain boundary sliding during the compression test.

Bicrystal specimens were deformed using the high-temperature compression test system schematically illustrated in Fig. 3. Tests were conducted at 1450°C in air, using a constant strain rate of $\varepsilon = 2.1 \times 10^{-6}$ s^{-1}. In one sample, the compression test was interrupted when the stress levels reached 37.5 MPa, and the grain-boundary morphology was observed using an optical microscope. The same sample was then retested multiple times with tests halted when stress levels reached, 50, 100 and 137.5 MPa, successively, and the morphology of the same regions of the grain boundary were examined after each test to show the evolution of the structure with increasing strain. Other samples subjected to smaller stresses and with smaller strains were examined by transmission electron microscopy.

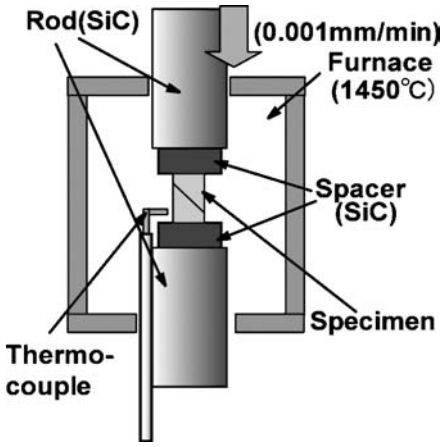

Figure 3 Schematic of high-temperature compression test system employed in this study. Tests were conducted at 1450°C in air, using a constant strain rate of $\varepsilon = 2.1 \times 10^{-6}$ s^{-1}.

2.3. TEM observations

The grain-boundary structure was assessed using HRTEM. Specimens were mechanically polished to the thickness of less than 20 μm before ion thinning. Ion thinning was performed using a Gatan Precision Ion Polishing System (PIPS^{TM}) operating at 4.0 kV with beam incidence at 2–4 degree. Since alumina is an electronic insulator, specimens were coated with a 3 nm thick carbon film using the Gatan Precision ion Etching Coating System (PECS^{TM}). HRTEM observations were performed with a Topcon EM-002B and a JEOL 4010 operating at 200 and 400 kV, respectively. The grain boundary was observed in a cross sectional view parallel to the [0001] direction.

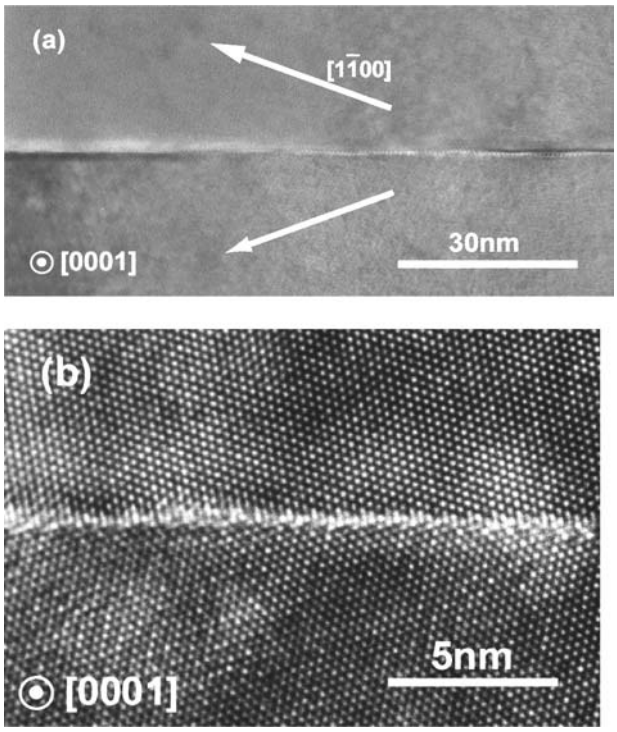

Figure 4 (a) HRTEM image of the $\Sigma 7\{4\bar{5}10\}$ boundary in an alumina bicrystal, and (b) the magnified image of the grain-boundary core structure. The beam direction was selected to be parallel to the [0001], and white spots in the image correspond to the aluminum columns. It is clearly seen that the two sapphire blocks were successfully joined at the atomic level.

3. Results and discussions

The grain boundary of the as-bonded alumina bicrystals contains no macroscopically detectable pores or defects. Figs 4a and b shows HRTEM images of the $\Sigma 7\{4\bar{5}10\}$ boundary viewed along the [0001] direction. White dots correspond to aluminum columns, and oxygen columns correspond to the centers of the triangles formed by the aluminum columns [29, 30]. No intergranular amorphous film was detected, and the two crystals were well bonded at the atomic level. From the analysis of the HRTEM image, it was determined that the tilt angle in the bicrystal was 38.2°, which differed by $<1^\circ$ from ideal crystallographic misorientations. The "as-bonded" grain boundary is relatively planar without large facets, although small nanoscale oscillations in the grain boundary position are typically observed as shown in Fig. 4a.

Fig. 5 shows a series of optical micrographs of the deformed grain boundary at its line of intersection with the (0001) planes of the sapphire blocks. In these micrographs, the "horizontal" line is the grain boundary and the lines at about 45° to the grain boundary are the scratches introduced to detect the extent and uniformity of grain boundary sliding. All images were taken from the same region along the grain boundary after stressed at (a) 37.5 MPa, (b) 50 MPa, (c) 100 MPa and (d) 137.5 MPa, respectively. The corresponding strains of the specimen were (a) 0.6% (b) 0.7% (c) 1.1% and (d) 1.3%. The direction of the shear stress is indicated in Fig. 5a. Examination of the scratches on both sides of the grain boundary suggests little grain boundary sliding. However,

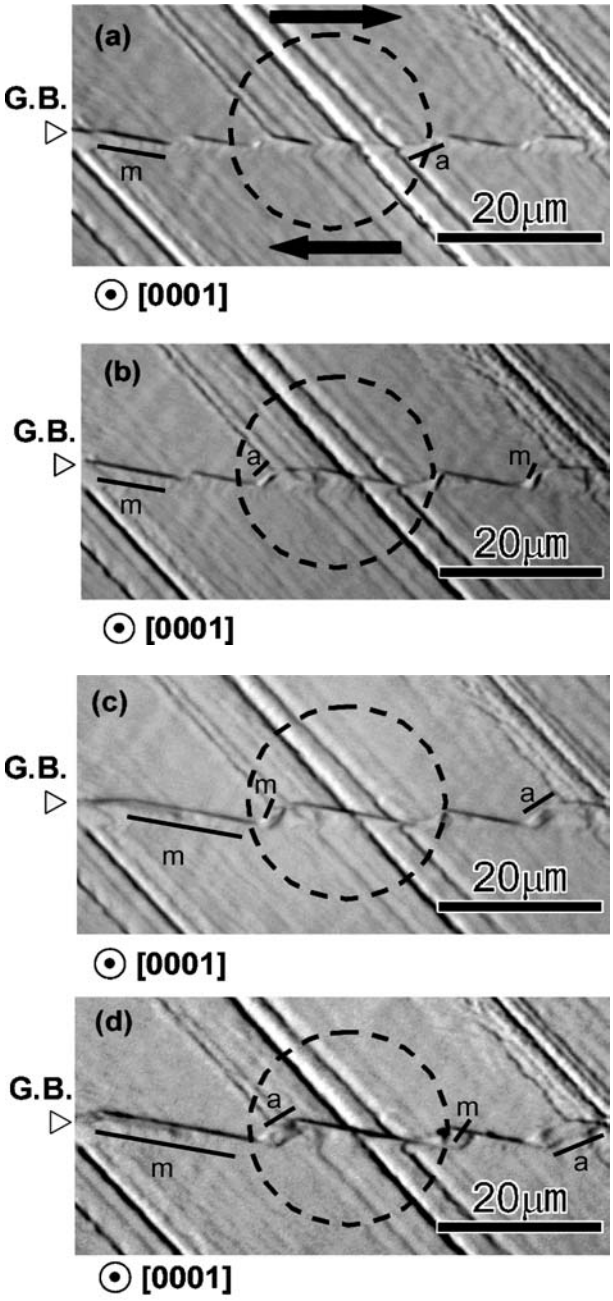

Figure 5 A series of optical micrographs of the deformed grain boundary. Applied stresses were (a) 37.5, (b) 50, (c) 100, and (d) 137.5 MPa, respectively. Shear stress was applied in the direction indicated by arrows in (a). The scratched lines are intentionally introduced on the polished surface for detecting the extent and uniformity of sliding. These images were taken from the same area of the specimen. The grain boundary did not show a significant shear displacement, but clearly faceted.

with deformation the initially planar grain boundary evolves into a structure composed of two distinct facets, both inclined to the original $\Sigma 7\{4\bar{5}10\}$ grain boundary plane.

Fig. 6 shows an atomistic model of the initial $\Sigma 7\{4\bar{5}10\}$ grain-boundary structure, which was calculated by the static lattice calculation in our previous study [29, 30]. The GULP code was used for the calculation [31]. From the facet orientations in Fig. 5, the facets appear to correspond to low-index planes of the two adjoining alumina grains. The longer facets appear to lie parallel to the m-plane of the lower crystal, and the shorter more steeply inclined facets lie nearly parallel

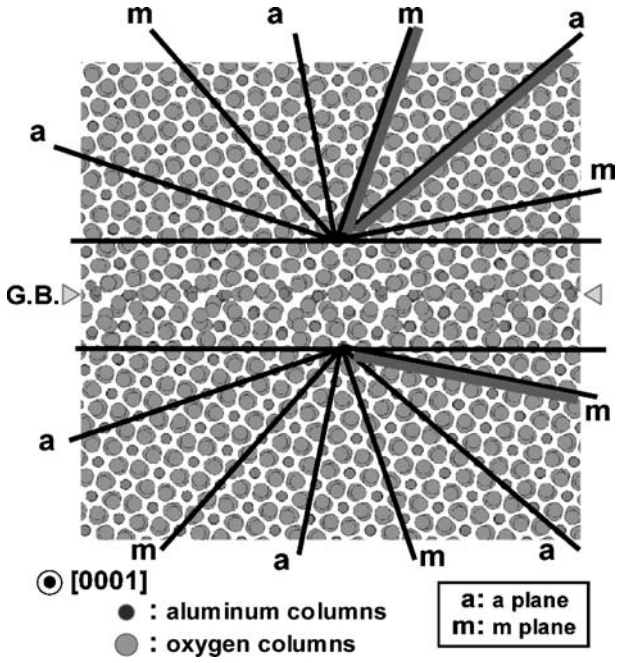

Figure 6 An atomistic model of the initial $\Sigma7\{45\bar{1}0\}$ grain-boundary structure calculated in our previous study [29, 30]. The grain boundary lies horizontally in the middle of the figure. "m" and "a" represent *m*-plane and *a*-plane, which are low-index planes in alumina. From the facet orientations in Fig. 5, the faceted planes appear to correspond to the low-index planes of adjoining grains.

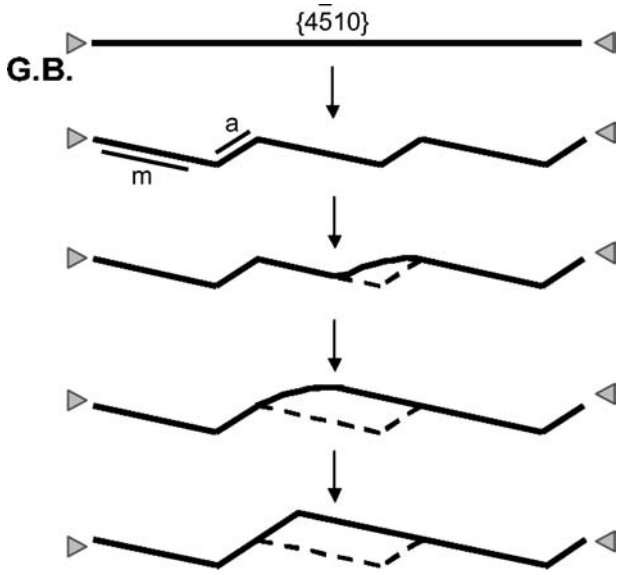

Figure 7 Schematic of facet coarsening process observed inside the circled regions in Fig. 5.

to the a-plane of the lower crystal and the m-plane of the upper crystal.

Coarsening of the facet structure during deformation is also evident in Fig. 5. Fig. 7 shows a schematic representation of the facet coarsening as suggested by microstructural changes inside the circled regions in Fig. 5. Facets grew due to the migration of selected short facets along the longer facets until the entire facet was traversed. Ledge migration is associated with a temporary rounding of sections along the boundary, and the disruption of the facet may facilitate the atomic exchanges involved in ledge displacement.

The observation of coarsening involving facets that were microns in length, and the absence of obvious facets in as-bonded samples (produced with only a small contact load) encouraged TEM examination of more lightly deformed samples. It was hoped that such a sample would provide information on finer-scale faceting and facet nucleation. Studies were therefore performed on an identical $\Sigma7\{45\bar{1}0\}$ alumina bicrystal compressed by 0.2% (maximum stress 6.3 MPa) at 1450°C in air using the same strain rate employed in the earlier experiment. After deformation, the grain boundary was observed using both optical and transmission electron microscopy.

Fig. 8 shows an optical micrograph of the grain boundary region in a slightly deformed bicrystal. At this resolution, the grain boundary appears to be planar, suggesting that the $\Sigma7\{45\bar{1}0\}$ interface is stable. Figs 9a and b show TEM images of the grain boundary region in the same lightly deformed alumina bicrystal. Comparing images in Figs 4a and 9a, taken at the same magnification, deformation induced changes in the topography of the interface are apparent. The grain

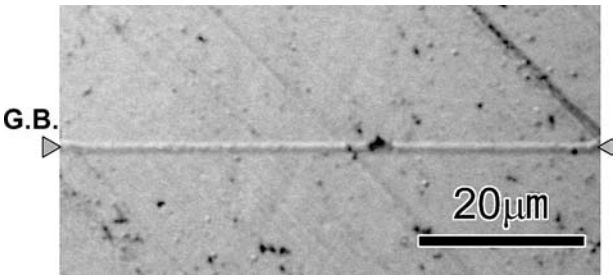

Figure 8 Optical micrograph of the slightly deformed grain boundary. Applied stress was 6.3 MPa. The grain boundary appears to be planar at this resolution.

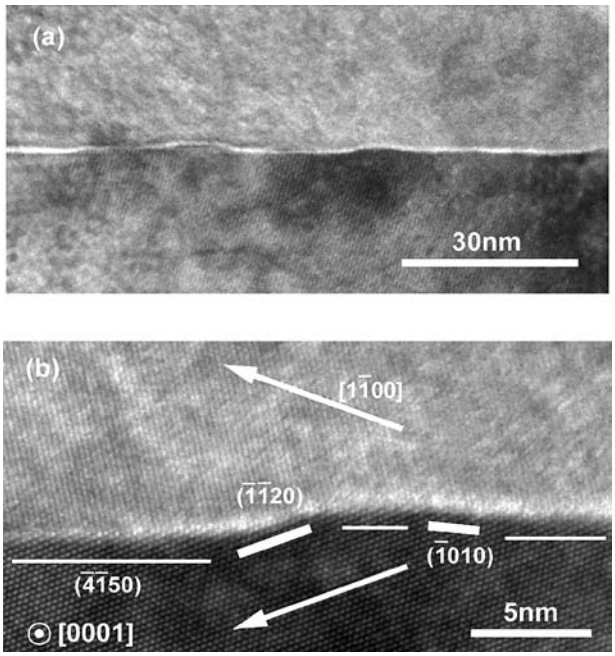

Figure 9 (a) TEM images of the slightly deformed (6.3 MPa) grain boundary. The grain boundary became way as a result of deformation. (b) Magnified image of the wavy area in (a). This image suggests the formation of multiple small low-index facets with multiple low-index planes.

boundary has shifted off the initial $\{4\bar{5}10\}$ boundary plane, has periodic waves, suggesting fine-scale or insipient ledge formation. Fig. 9b provides a higher magnification image of a portion of the region shown in Fig. 9a. The HRTEM image suggests the formation of a small inclined facet oriented parallel to the $\{\bar{1}\bar{1}20\}$ plane of the lower crystal. An image taken along the [0001] is only sufficient to establish the index as $\{\bar{1}\bar{1}2x\}$, however, the $\{\bar{1}\bar{1}20\}$ surface planes are stable [32, 33] Rödel and Glaeser [34] suggested that grain boundary planes lying parallel to stable low-index surfaces could facet even in the absence of intergranular films due to grain boundary torque terms, and recent work by Park [35] provides some validation of this suggestion. Since the $\{10\bar{1}0\}$ surface plane is unstable in alumina, inclined facet planes with edges that appear to lie parallel to the $\{10\bar{1}0\}$ plane may be composed of even finer-scale $\{\bar{1}\bar{1}20\}$ facets, or may be the surface trace of $\{10\bar{1}x\}$ surfaces. These nanoscale facets are thought to be the origin of the micron-scale facets evident at larger strain, and may coarsen by the same mechanism described previously.

To fully understand facet development, the process leading to the initial formation of $\{\bar{1}\bar{1}20\}$ plane facets needed to be clarified. The facets are not present in the as-bonded crystal, even though the bonding temperature (1500°C) exceeds the deformation temperature (1450°C) and the bonding time (10 h) exceeds the deformation test duration. If the $\Sigma7\{4\bar{5}10\}$ boundary is inherently unstable one might expect that it would decompose to a more stable faceted structure during the bonding cycle. Instead, stress plays a key role initiating this breakup. Whether it changes the energetics or simply aids in overcoming a nucleation barrier to reorienting the interface is unknown. One possibility is that the reorientation of the interface during deformation, the interfacial rumpling evident in Fig. 9 drives the interface out of a local energy minimum in which the stable plane is oriented parallel to the $\{4\bar{5}10\}$ planes of the adjoining crystals. The rumpling allows the interface orientation to transition to an adjoining energy minimum, one associated with pairs of inclined facets. Once inclined facets are formed, the migration processes described lead to a gradual coarsening of the structure, and an energy barrier prevents the faceted interface from "smoothing" and restoring the original $\{4\bar{5}10\}$ boundary plane.

The process of atomic shuffling associated with reorientation of the boundary plane is schematically described in Fig. 10. Dotted lines represent the lattice of the upper crystal and solid lines indicate the lattice of lower crystal. The smaller superimposed lattice in Fig. 10 corresponds to the DSC (displacement shift complete) lattice for this grain boundary. Circles and squares represent the positions of aluminum columns in the lower and upper crystals, respectively. The initial grain boundary is represented by the thick horizontal line in Fig. 10a. When the columns of Al atoms represented by the highlighted square points shift to the lattice points for Al atoms in the lower crystal (indicated by small arrows), the grain boundary plane can reorient as shown in Fig. 10b. Fig. 10c shows another variation in which small atomic displacements "nucleate" a more steeply inclined facet. The DSC vectors in Fig. 10 are (b) $1/21[\bar{1}3\bar{2}0]$, $1/21[\bar{2}\bar{1}30]$, $1/21[\bar{1}3\bar{2}0]$ (c) $1/21[3\bar{2}\bar{1}0]$, $1/21[\bar{3}210]$ and $1/21[\bar{2}\bar{1}30]$ (from left to right). Rumpling of the boundary due to stress may simplify such a reorientation of the interface and allow it to occur over larger dimensions. An experiment, in the misorientation angle is preserved but the grain boundary plane is systematically varied, could be very useful in shedding further light on the energetics and kinetics of faceting. Anneals of such samples in their as-bonded condition may show that when the grain boundary plane deviates by more than some critical angle from the $\Sigma7\{4\bar{5}10\}$ boundary plane, equilibrium configurations involving the formation of inclined facets occur. Such experiments could potentially verify the suggested energetic arguments for the facet development, and pinpoint the role of the deformation in triggering this faceting and reorientation of the boundary plane.

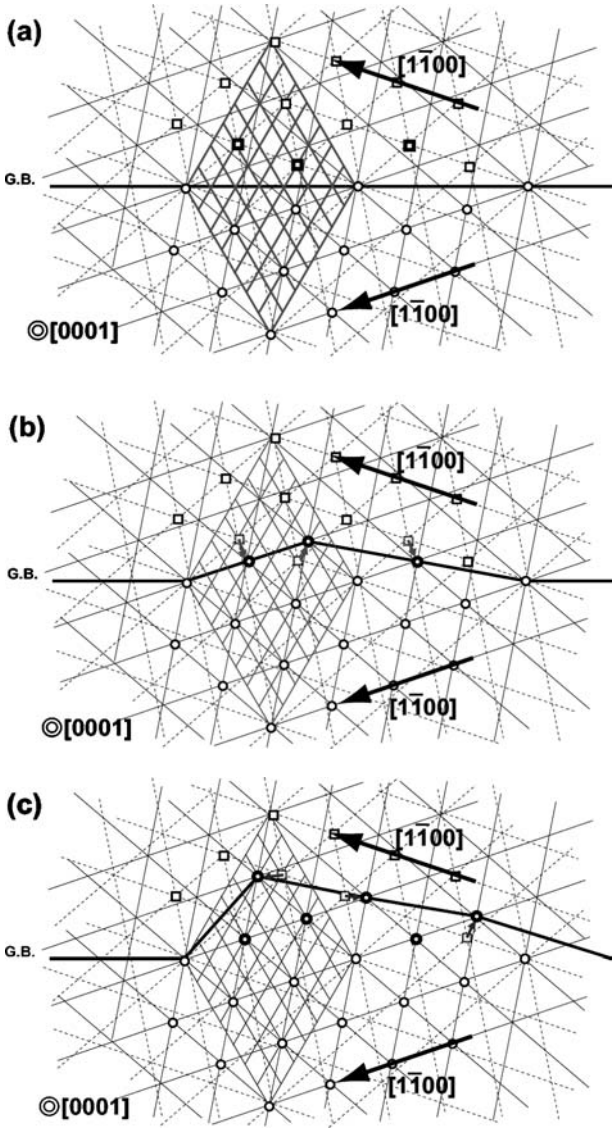

Figure 10 Schematics of CSL-DSC plots for a $\Sigma7\{4\bar{5}10\}$ grain boundary in alumina. Dotted lines represent the lattice of the lower crystal, and solid lines that of the upper crystal. A smaller lattice in the center is the DSC lattice of this specific $\Sigma7$ boundary. (a) Initially straight grain boundary, and (b) the grain boundary that has been shifted by small atomic displacements. The atoms on the square sites shift to circle sites. As shown in (c), additional atomic shuffling can grow low-index facets.

4. Summary

Constant strain rate compression tests at 1450°C were performed on a $\Sigma 7\{4\bar{5}10\}$ alumina bicrystal. The morphology of the grain boundary before and after the sample was strained was examined at optical and atomic resolution.

(1) The introduction of stress in the bicrystal caused the $\Sigma 7\{4\bar{5}10\}$ boundary plane to evolve into two inclined facets oriented parallel to low index directions within the adjoining crystals. The facet lengths increased and the facet density decreased with increasing strain. Facet coarsening was observed to involve the migration of what appear to be smoothly rounded segments parallel to the long facets. Deformation may cause a temporary breakup of the facet.

(2) TEM observation on a lightly deformed bicrystal showed that rumpling of the interface occurred and HRTEM indicated the development of facets oriented parallel to *a*-plane. The absence of dislocations in the adjoining grain suggests that the stress can occur facet only by enhancing diffusion without any dislocations.

Acknowledgements

This study was supported by a Grant-in-Aid for Scientific Research and Special Coordination Funds from the Ministry of Education, Culture, Sports, Science and Technology, and Japan Society of Promotion of Science (JSPS), Japan.

References

1. R. RAJ and M. F. ASBHY, *Metall. Trans.* **2** (1971) 1113.
2. R. M. CANNON, W. H. RHODES and A. H. HEUER, *J. Am. Ceram. Soc.* **63** (1980) 46.
3. T. WATANABE, M. YAMADA, S. SHIMA and S. KARASHIMA, *Phil. Mag. A* **40** (1979) 667.
4. R. MONZEN, Y. SUMI, K. KITAGAWA and T. MORI, *Acta Metall. Mater.* **38** (1990) 2553.
5. A. D. SHEIKH-ALI and J. A. SZPUNAR, *Mater. Sci. Eng. A* **245** (1998) 49.
6. C. SCHMIDT, M. W. FINNIS, F. ERNST and V. VITEK, *Phil. Mag. A* **77** (1998) 1161.
7. J. R. HU, S. C. CHANG, F. R. CHEN and J. J. KAI, *Mater. Chem. Phys.* **74** (2002) 313.
8. D. G. BRANDON, B. RALPH, S. RANGANATHAN and M. S. WALD, *Acta Metall.* **12** (1964) 814.
9. D. A. SMITH and R. C. POND, *Int. Metals. Rev.* **205** (1976) 61.
10. T. WATANABE, Y. IKUHARA and T. SAKUMA, *J. Ceram. Soc. Jpn.* **106** (1998) 888.
11. Y. IKUHARA, T. WATANABE, T. SAITO, H. YOSHIDA and T. SAKUMA, *Mater. Sci. Forum.* **294–296** (1999) 273.
12. Y. IKUHARA, T. WATANABE, T. YAMAMOTO, H. YOSHIDA and T. SAKUMA, in "Ceram. Trans." (American Ceramic Society, Westerville, OH, 2000) Vol. 18, pp. 293.
13. P. R. KENWAY, *J. Am. Ceram. Soc.* **77** (1994) 349.
14. F. R. CHEN, C. C. CHU, J. Y. WANG and L. CHANG, *Phil. Mag. A* **72** (1995) 529.
15. S.-D. MO, W.-Y. CHING and R. H. FRENCH, *J. Am. Ceram. Soc.* **79** (1996) 627.
16. S. FABRIS and C. ELSÄSSER, *Phys. Rev. B: Condens. Mater.* **64** (2001) 1.
17. T. HÖCHE, P. R. KENWAY, H.-J. KLEEBE and M. RÜHLE, *J. Am. Ceram. Soc.* **77** (1994) 339.
18. S. NUFER, A. G. MARINOPOULOS, T. GEMMING, C. ELSÄSSER, W. KURTZ, S. KOSTLMEIER and M. RÜHLE, *Phys. Rev. Lett.* **86** (2001) 5066.
19. A. G. MARINOPOULOS and C. ELSÄSSER, *Acta Mater.* **48** (2000) 4375.
20. N. SHIBATA, T. YAMAMOTO, Y. IKUHARA and T. SAKUMA, *J. Electron. Microsc.* **50** (2001) 429.
21. N. SHIBATA, N. MORISHIGE, T. YAMAMOTO, Y. IKUHARA and T. SAKUMA, *Phil. Mag. Lett.* **82** (2002) 175.
22. N. SHIBATA, F. OBA, T. YAMAMOTO, T. SAKUMA and Y. IKUHARA, *Phil. Mag.* **83** (2003) 2221.
23. H. YOSHIDA, K. YOKOYAMA, N. SHIBATA, Y. IKUHARA and T. SAKUMA, *Acta Mater.* **52** (2004) 2349.
24. Z. G. MAO, S. B. SINNOTT and E. C. DICKEY, *J. Am. Ceram. Soc.* **85** (2002) 1594.
25. W.-Y. LEE, P. D. BRISTOWE, Y. GAO and K. L. MERKLE, *Phil. Mag. Lett.* **68** (1993) 309.
26. U. DAHMEN, S. PACIORNIK, I. G. SOLORZANO and J. B. VANDERSANDE, *Inter. Sci.* **2** (1994) 125.
27. D. M. SAYLOR, A. MORAWIEC, B. L. ADDAMS and G. S. ROHRER, *ibid.* **8** (2000) 131.
28. K. L. MERKLE and D. J. SMITH, *Phys. Rev. Lett.* **59** (1987) 2887.
29. K. MATSUNAGA, H. NISHIMURA, T. SAITO, T. YAMAMOTO and Y. IKUHARA, *Philo. Mag.* **83** (2003) 4071.
30. H. NISHIMURA, K. MATSUNAGA, T. SAITO, T. YAMAMOTO and Y. IKUHARA, *J. Am. Ceram. Soc.* **86** (2003) 574.
31. J. D. GALE, "GULP (General Utility Lattice Program)" (Royal Institution of Great Britain, London, U.K., 1993).
32. J.-H. CHOI, D.-Y. KIM, B. J. HOCKEY, S. M. WIEDERHORN, C. A. HANDWERKER, J. E. BLENDELL, W. C. CARTER and A. R. ROOSEN, *J. Am. Ceram. Soc.* **80** (1997) 62.
33. M. KITAYAMA and A. M. GLAESER, *ibid.* **85** (2002) 611.
34. J. RÖDEL and A. M. GLAESER, *ibid.* **73** (1990) 3292.
35. C. W. PARK, D. Y. YOON, J. E. BLENDELL and C. A. HANDWERKER, *ibid.* **86** (2003) 603.

Received 9 September 2004
and accepted 31 January 2005